EFFECTS OF WOOD ANATOMY ON THE MECHANICAL BEHAVIOR OF SINGLE-BOLTED CONNECTIONS

Audrey Zink-Sharp

Associate Professor
Department of Wood Science and Forest Products
Virginia Tech
Blacksburg, VA 24061-0323

John S. Stelmokas

Chemist
Kanzaki Speciality Papers
Ware, MA 01082-2002

and

Hong-mei Gu

Graduate Research Assistant
Department of Wood Science and Forest Products
Brooks Forest Products Center
Virginia Tech
Blacksburg, VA 24061-0503

ABSTRACT

This study combined mechanical testing of full-size bolted connections, determination of microme-chanical properties of individual growth rings within the full-size specimens, and video microscopy for anatomical and mechanical measurements. Hard maple (*Acer* spp.) and northern red oak (*Quercus rubra*) specimens representative of single-bolted connections were tested to failure in bearing stress and analyzed using video microscopy methods. Maximum crushing strength of individual growth rings was obtained from specimens that were 1 mm × 1 mm in cross section and 4 mm along the grain. Anatomical measurements of cell-wall thickness, percent vessels in a given area, and ray width were obtained for each species and correlated to failure mode. It was concluded that maple had a consistent failure mode, while oak had a variable failure mode. The difference in failure modes is attributed to the different anatomical structures of the two species, mainly, ray and vessel size. Bearing stress was not statistically significantly influenced by the different anatomical features; however, stiffness in compression was.

Keywords: Bearing stress, bolted timber connections, failure mode, micromechanical properties, video microscopy.

INTRODUCTION AND BACKGROUND

The mechanical behavior of bolted wood connections under load is very complex and is influenced by many variables. Our knowledge of this behavior is based largely on macroscopic observations. The behavior of a single-bolted connection loaded parallel to the grain is relatively well known; however, most published research has focused on Douglas-fir or spruce and the results are extrapolated to other species through analytical or empirical models. Relatively few experiments have included hardwood species (Trayer 1932; Lheude 1987; Hilson et al. 1987) and no published studies are found that investigated the influence of wood anatomy on the failure modes or bearing stress of bolted connections for either hardwoods or softwoods. However, the relationship of anatomy to compression failures parallel to the grain has been studied ex-

tensively (Kucera and Bariska 1982; Côté and Hanna 1983; Bariska and Kucera 1985; Choi et al. 1996, among others).

Several experimental techniques have been utilized to study the stresses and strains in the neighborhood of a loaded bolt hole. Strain gages and moire interferometry have been the traditional techniques (Wilkinson and Rowlands 1981; Rowlands et al. 1982; Rahman et al. 1991). Humphrey and Ostman (1989 a, b) have developed techniques to model wood deformation around bolts and to study bending and overall displacement of bolts within connections. In their studies, a steel pin is passed through thin wood wafers and the associated wood deformation is photographed. They also utilized X-ray scans to quantify the bending and overall displacement of a single bolt within a joint. When the X-ray technique was combined with the wafer study, performance of both the wood and the bolt could be evaluated. The techniques of Humphrey and Ostman (1989 a, b) were used by Fantozzi and Humphrey (1995) to study multiple bolt connection behavior. Their results indicate that these methods could be helpful in designing new joint configurations and determining the influence of certain wood variables; however, the technique has not been applied to full-size connections. Single-beam reflection holography was used by Kermani and McKenzie (1994) to study the effects of grain angle on behavior of single-bolted connections in compression. Results for in-plane and out-of-plane displacements showed that strain distributions around the bolts were highly dependent on the grain orientations. Stelmokas et al. (1997) have used computer vision and image processing to determine displacement beneath bolts in multiple-bolted wood connections. This study used double-shear connections constructed of yellow-poplar. Five different bolt patterns were used to analyze the influence of number of bolts in a vertical row and in a horizontal column. It was discovered that for multi-bolt patterns in a vertical row, parallel to load displacements below the outer bolts were higher than those beneath the center bolt(s) but

not equal in magnitude as previously assumed. Salinekovich et al. (1996) used specially instrumented bolts to determine the influence of manufacturing imperfections on load sharing and assess the present design procedures for multi-bolted connections.

Prior to 1983, design for the strength of a single-bolted connection was based mainly on research conducted by Trayer (1932). Trayer's work consisted of a few joint geometries, and then the results were extended to a wide range of geometries and species. Later, European researchers developed an analytical joint strength model known as the Yield Theory, which was based on original work by Johansen (1949). The yield theory uses connection geometry and material properties to evaluate the strength of two- or three-member dowel-type connections. McLain and Thangjitham (1983) applied this theory to parallel-to-grain loading of bolted wood joints and found good agreement between predicted and experimental failure loads. Soltis et al. (1986) found that the yield theory predicted joint strength reasonably well for both parallel- and perpendicular-to-grain loading because it incorporated wood and bolt properties leading to a rational design approach. The 1991 National Design Specification for Wood Construction (AFPA 1991) incorporated yield theory in design of connections for laterally loaded dowel-type fasteners and it has been adopted by European communities for the EUROCODE Design System (Larsen 1992). However, present design specifications for bolted joints do not include influences of wood quality and anatomical features in the vicinity of connections on overall joint performance.

OBJECTIVES

Because of a lack of information on influences of anatomical features on failure modes and bearing stress of bolted timber connections, the limited number of species used in the studies, and the need for wood properties in the design codes for wood connections in the yield theory, the objective of this study

was to determine the influence of different hardwood anatomical features on the performance of bolted joints in hard maple (*Acer* spp.) and northern red oak (*Quercus rubra*). Specifically studied were: 1.) the failure mode, 2.) the bearing stress and joint stiffness in compression, and 3.) the micromechanical properties of individual growth rings.

Because the focus of this study was to examine the relationships between wood anatomy and mechanical behavior, it was desirable to minimize the effects of specific gravity. Red oak and hard maple were chosen because they have approximately the same specific gravity but yet have very different anatomical structures, and they will provide information on hardwoods that is currently lacking. As seen in Fig. 1a, red oak, which is a ring-porous species, has large conspicuous rays, and is highly variable in structure; maple, however, is diffuse-porous, has smaller rays, and is quite uniform in structure (Fig. 1b).

METHODS AND MATERIALS

Full-size bolt connections

Rough, flatsawn, $\frac{3}{4}$ red oak and hard maple boards were obtained from a local lumber supplier. The boards were chosen so that straight-grained specimens could be machined. Eighteen specimens (9 maple and 9 oak) were machined to the approximate final dimensions of 46 mm (1-$\frac{13}{16}$ in.) in thickness (radial direction), 102 mm (4 in.), in width (tangential direction), and 152 mm (6 in.) in length parallel to the grain. A 13.5-mm ($\frac{17}{32}$-in.) hole was drilled in the center of the wide face of each specimen (T-L face). The bolt was 12.7 mm ($\frac{1}{2}$ in.) in diameter. The specimen configuration is illustrated in Fig. 2. Moisture content (MC) and specific gravity (SG) were determined according to ASTM Standard D-2016-83 (ASTM 1986a) and ASTM Standard D-2395-83 (ASTM 1986b), respectively.

A two- or three-member connection is commonly used to analyze bolted connections in wood. However, this study was primarily concerned with examining failure mode and bearing stress of the center member in a three-member connection. To accomplish this, a special testing apparatus was constructed that is similar to a dowel-bearing strength test as recommended by ASTM D 1761 testing specifications (ASTM 1993). Figure 2 illustrates a diagram of the test fixture used for applying bearing loads. Specimens were loaded to failure at a constant crosshead rate of 1 mm/min (0.04 in./min). All specimens were tested at an average moisture content of 8–10%. Average specific gravity at test for the maple specimens was 0.63 and it was 0.57 for red oak. Average area of earlywood for the red oak specimens was 0.017 m^2 and 0.045 m^2 for the latewood portion. Failure was defined to be the first major drop in load. Load-displacement curves and maximum load data were obtained for each specimen.

Microscopic examination

After testing was complete, the failed specimens were visually examined to determine the failure mode with a stereo optical microscope. Then, for computer image analysis and quantification of the anatomy, small 13-mm × 13-mm ($\frac{1}{2}$-in. × $\frac{1}{2}$-in.) blocks near the bolt holes were cut from various specimens (not including the failed zones) so that light microscope slides could be prepared. These blocks included growth rings that were representative of those observed in the failed zones. Blocks were immersed in water, a vacuum was applied, and they were allowed to soak overnight to soften for better microtome slicing. A sliding microtome was used to obtain thin sections from the wood blocks. The thin sections were stained with fast green and Safranin stains to accentuate cellulose and lignin, respectively, and then mounted on glass microscope slides. Microscopic measurements were made on cell-wall thickness, number of vessels and cell-wall thickness per unit area, and ray width of each species with the computer software to correlate with the observed failure modes.

Micromechanics specimens

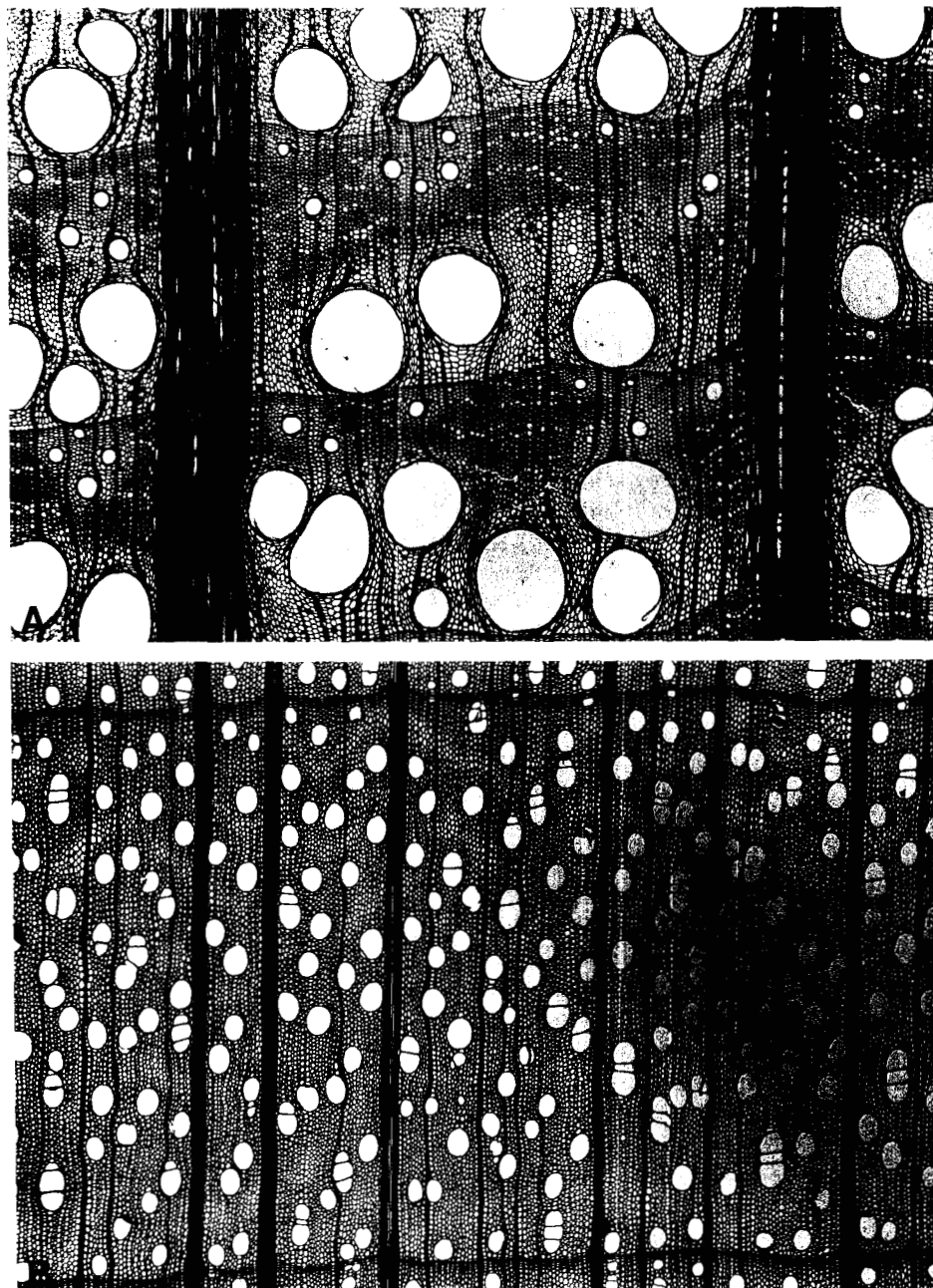To determine the correlation of the failure modes with individual growth ring behavior,

FIG. 1.   Illustration of cross-sectional wood anatomy. 45×. 1a) red oak (*Quercus rubra*) illustrating ring porosity and wide rays. 1b) maple (*Acer* spp.) illustrating diffuse porosity and narrow rays.

micromechanics test specimens were prepared from several locations in the full-size test specimens. The locations were chosen at random and distant from both the specimen ends and the bolt hole. Ten micromechanics specimens were prepared from the maple blocks, ten were prepared from the earlywood (EW) portions of the red oak blocks and ten from
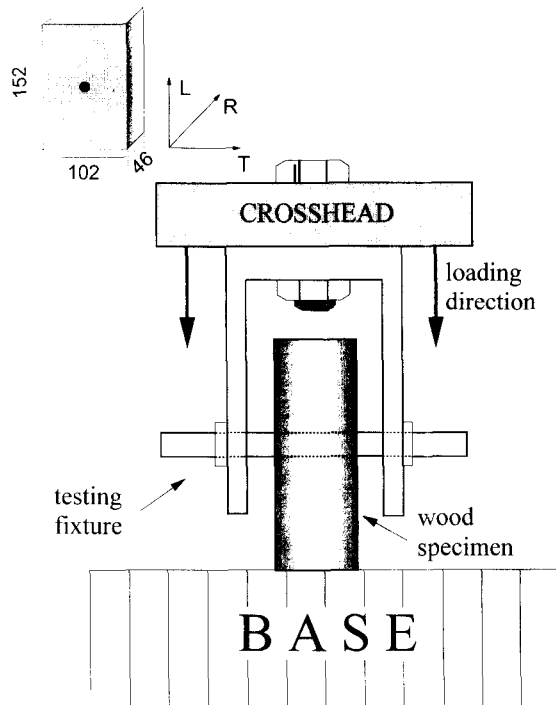
Fig. 2. Diagram of test specimen (inset in upper left) and test fixture for applying the bearing load to the full-size specimens. All dimensions are mm.

latewood (LW) portions. Average dimensions were 1 mm × 1 mm in cross section and 4 mm along the grain (0.034 in. × 0.034 in. × 0.160 in.). Average moisture content at test for the maple microspecimens was 9%, oak earlywood was 13%, and oak latewood was 15%. Specific gravity at test was 0.59 for the maple, 0.46 for oak EW, and 0.65 for oak LW. Compression tests were conducted using a Fullam microtesting device illustrated in Fig. 3 equipped with a 11.4 kg (25 lb) load cell. Load was applied at a constant crosshead rate of 0.003 mm/min (0.00012 in./min). Displacement (change in length of the specimen) was measured using video microscopy of computerized images acquired before and during the loading according to principals and techniques as fully described in Zink et al. (1995). Fig. 4 illustrates the complete set-up for micromechanical testing.

RESULTS AND DISCUSSION

Failure modes

The two main failure modes that were identified from examination of the failure test specimens were buckling failures and crushing failures. Buckling refers to a folding or wrinkling of the surface where the failure lines in the wood were at an angle to the grain direction. Crushing refers to a telescopic shortening or compression of the wood surface underneath the loaded area. A typical crushing failure of one of the maple specimens is shown in Fig. 5a, a typical buckling failure exhibited in the earlywood portion of red oak specimens is shown in Fig. 5b, and Fig. 5c illustrates a typical crushing failure observed in oak latewood. For other examples of buckling and crushing failures, see Bodig and Jayne (1982), Côté and Hanna (1983), and Bariska and Kucera (1985).

All maple specimens displayed a crushing type failure underneath the bolt hole as seen in Fig. 5a. The crushed area was remarkably uniform in visual character for all specimens examined. The only difference within the maple specimens was the relative expanse of the crushed area. However, on a macroscopic scale, there were no discernible differences. There are two possible reasons for the tendency to fail uniformly in crushing. As seen in Fig. 1b, maple has a very uniform diffuse-porous anatomical structure, and this uniformity in structure should result in uniformity in failure patterns. A homogeneous failure form throughout the growth rings of axial compression specimens of aspen was also observed by Kucera and Bariska (1982). In part 2 of their study (Bariska and Kucera 1985), they observed that the lack of density contrast within growth rings tended to produce less inclined failure planes, which are indicative of crushing rather than buckling failures. However, in an ultrastructure study of compression parallel-to-grain failures of ring and diffuse-porous hardwoods, Côté and Hanna (1983) observed no visible differences in the failure patterns. The second reason for the crushing failures
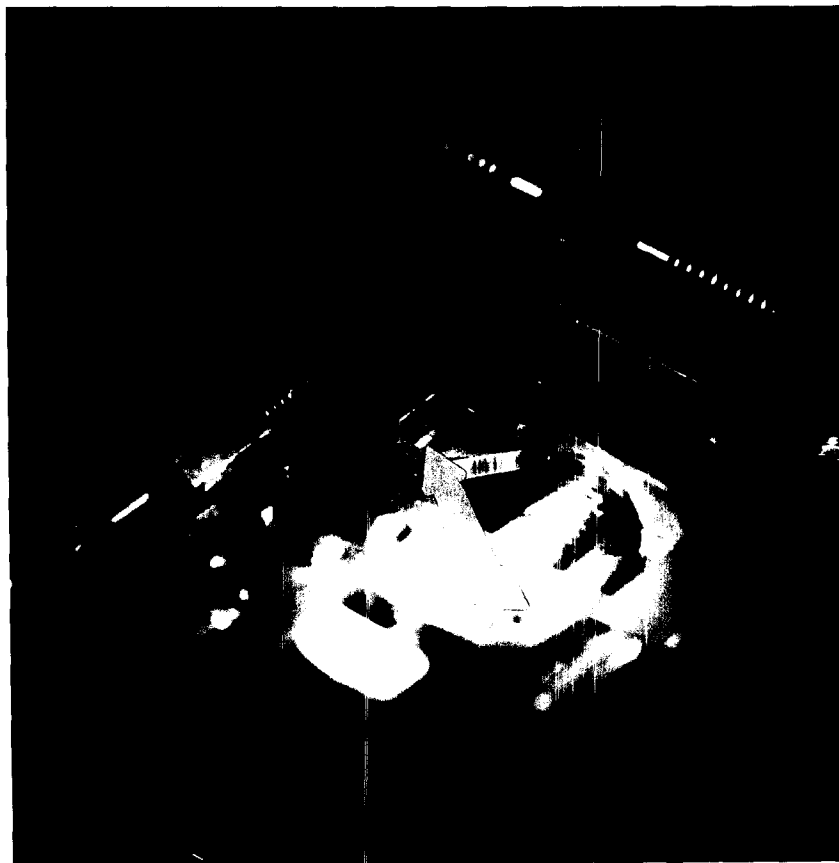
FIG. 3.   Close up of microtesting device, arrow indicates microspecimen inside testing fixture.

observed in the maple specimens is that the fiber cell elements in maple are generally strong, thick-walled, short columns, which when loaded, should fail in total compression, not buckling. These fibers also act to laterally support the weak, thin-walled vessels and thus cause them to fail in pure compression. Kucera and Bariska (1982) observed that fibers in aspen compression specimens exhibited telescopic shortening and folds; however they further observed that cell elements with narrow lumens such as latewood vessels and fibers also buckled.

The tendency of individual cells or groups of cells such as annual rings to crush rather than buckle is further understood in view of the slenderness ratio

$$L/D \qquad\qquad (1)$$

where

L = the length of the specimen beneath the bolt (69 mm)

D = the thickness of the test specimen or portion of annual ring in contact with the bolt.

Columns with slenderness ratios greater than 11 are considered long columns and should be expected to buckle under axial compression loads (Bodig 1965). In the case of the maple which is diffuse-porous, the whole specimen acts together, and the L/D ratio is 1.5, where L = 69 mm (2.7 in.) and D is 46 mm (1-$^{13}/_{16}$ in.). A slenderness ratio this low means that
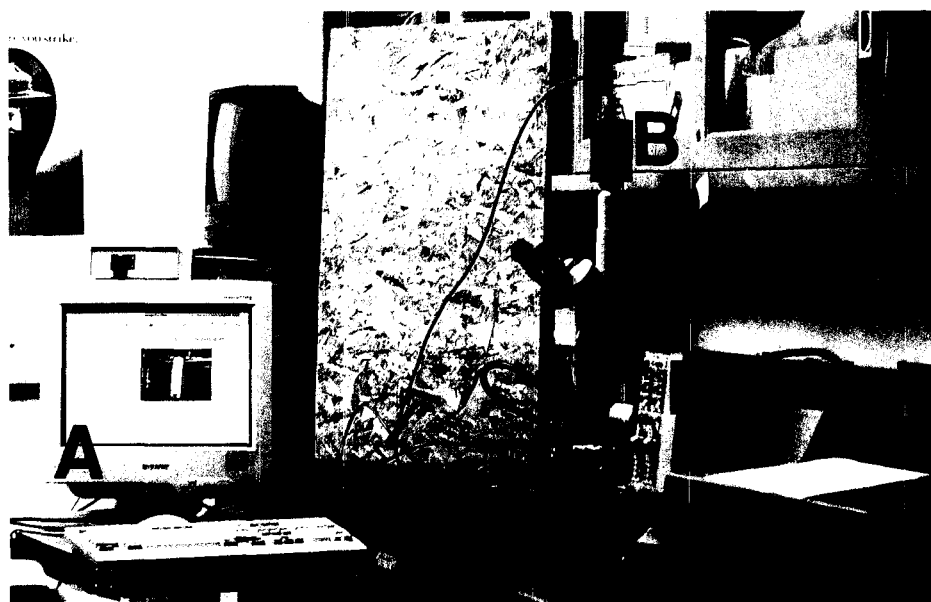
FIG. 4. Photograph of micromechanical test set-up; A—Image analysis computer, B—CCD Video Camera, C—Reflected light microscope, D—Microtesting device, E—Load signal conditioner, F—Chart recorder.

the specimen will tend to behave like a very short column and crush rather than buckle (Bodig 1965).

The oak specimens displayed two distinct failure modes depending on whether or not EW or LW was observed on the lateral surfaces. A buckling type failure was observed in the EW underneath the bolt hole (see Fig. 5b) and a crushing type failure was observed in the LW (Fig. 5c). The buckling folds were parallel to the tangential direction and at an average inclination angle of 45° to the grain. Ring-porous hardwoods may be considered a two-phase laminate of alternating large, thin-walled hollow tubes in the earlywood and stronger, thick-walled columns in the latewood (refer to Fig. 1a). The buckling failure observed in the EW occurred because the EW vessels, which are analogous to large, thin-walled tubes, provide little or no support along the sides when loaded in compression, and are unstable and buckle as a result. The crushing failure observed in the LW occurred because the LW is composed mostly of strong, thick-walled fibers as seen in Fig. 1b, which behave in a similar fashion to short, solid columns.

These thick-walled fibers also act to support the LW vessels. When loaded in compression, the fibers and LW vessels will fail in pure compression and not buckle. Those specimens exhibiting a transition zone between EW and LW displayed a combination of buckling and crushing failures with the EW exhibiting buckling failures and the LW, crushing failures. Bariska and Kucera (1985) observed that the compression specimens with distinct density contrasts within growth rings exhibited distinctly different failure patterns for EW versus LW and that these specimens displayed high angle inclination failure planes, and buckling failures as a result.

As with the maple specimens, the failure modes are further understood from the slenderness ratios. For the ring-porous red oak, the latewood bands will act like spaced columns (Bodig 1965), and the width of the latewood or earlywood bands in contact with the bolt will determine the slenderness ratios for that portion of the loaded cross section. For the entire EW portion of one oak specimen, the slenderness ratio of EW under load is 5.5 (L = 69 mm (2.7 in.) and D = 12.7 mm (0.5 in.))
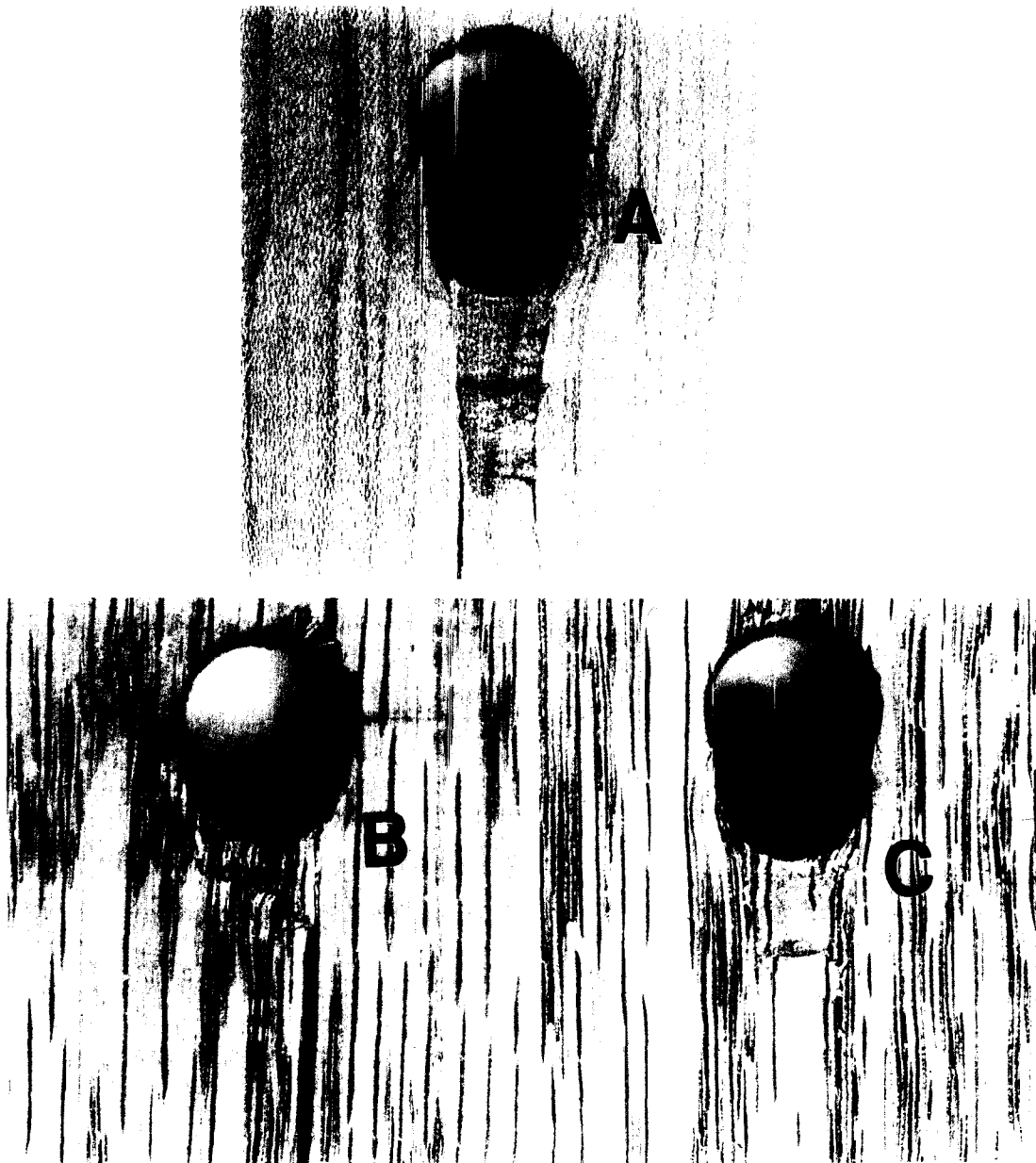
FIG. 5.   Photographs of typical failure modes in full-size bolt specimens. 2.25×. 5a) *crushing* failure observed in maple samples. 5b) oak displaying *earlywood buckling*. 5c) oak displaying *latewood crushing*.

and for the entire LW portion, it is 2.1 (L = 69 mm (2.7 in.) and D = 33.3 mm (1.31 in.)). For an *individual column* of EW, the ratio is 87 (L = 69 mm (2.7 in.) and D = 0.79 mm (0.03 in.)) and for an *individual LW column*, it is 30 (L = 69 mm (2.7 in.) and D = 2.3

mm (0.09 in.)). The much higher slenderness ratios for the EW portions of the specimen would indicate that this part of the specimen would buckle rather than crush and the LW would tend to crush. Because the growth rings are continuous across the area in contact with

the bolt, it is probable that a direct interpretation of these slenderness ratios calculated from individual columns of EW supported by LW cannot be made, but the ratios can serve as a useful guide (Bodig 1965).

All oak specimens displayed numerous small or large cracks above and below the bolt hole. Most cracks occurred within a ray or were initiated near a ray. The influence of multiseriate rays or ray margins in either initiation or serving as crumble zones was also observed by Schniewind (1959), Kucera and Bariska (1982), Bariska and Kucera (1985), Côté and Hanna (1983), and Choi et al. (1996). The initiation of cracks near the rays can be explained by the Poisson effect, the disruption of the longitudinal organization caused by the lateral ray, low tension perpendicular-to-grain strength, and lower fracture toughness values. When the bolt was loaded, the Poisson effect dictates that the material will expand in a direction that is perpendicular to the force direction, thus causing tension perpendicular to the grain in the specimens. The perpendicular tension leads to separation of the wood in the form of cracks at the weakest point in the specimen, which for the red oak is the rays. The large, multiseriate rays of oak represent a plane of weakness or potential stress concentrator because, when loaded perpendicular to their long axis, they are not as strong as longitudinal fibers and will collapse. Further, they cause a disturbance in the regular, longitudinal alignment of the majority of the cell elements. Cracking was more prolific in red oak due in part to differences in tension perpendicular strength and Mode I fracture toughness. Values for Mode 1 (opening mode) TL crack alignment for air-dry red oak is 407 $kN/m^{3/2}$ and for air-dry hard maple, 492 $kN/m^{3/2}$ (Bodig and Jayne 1982). Tension perpendicular-to-grain maximum strength for air-dry red oak is 5.5 MPa and for air-dry hard maple is 16 MPa. (USDA Wood Handbook 1987). Transfer of tension stresses perpendicular to the grain has also been observed by Humphrey and Ostman (1989a) and in the numerical analysis of Wong and Matthews (1981).

While the failure patterns in the maple were consistent for all specimens, no two oak specimens were alike. This is probably a result of the variability in the annual ring structure in the oak specimens as illustrated in Fig. 1a. The only similarity that was observed between the maple and oak specimens was that the oak LW regions failed in almost the same manner of crushing as the maple specimens. This is not unexpected since both are composed mainly of strong, thick-walled fibers and thus much more cell-wall material than the oak EW region. It appears, then, that the observed failure mode depends on the amount of cell wall material.

Microscopic measurements of cell elements

Based on the gross observations as discussed in the previous section, it was determined that the amount of solid cell-wall material relative to open lumen space in a given region and the width of the rays were the primary factors influencing the observed failure modes. These factors were quantified using computer vision and image processing (Umbaugh 1998) of the ray width, cell-wall thickness, percent cell-wall material, and percent vessel space. Percent cell-wall material is the percentage of solid cell-wall material in a given area and, likewise, percent vessel area is a measure of the amount of space in a given area occupied by vessels. A summary of the measurements is shown in Table 1. Average values were calculated from 50 measurements of each anatomical feature. Volumetric composition of northern red oak and sugar maple is included in this table to illustrate the percentages of the various cell elements.

The primary cell elements that contribute to the amount of lumen space are vessels (Panshin and de Zeeuw 1980). Therefore, the assumption behind our measurements was that whatever is not occupied by vessel lumen space must be occupied by mostly cell-wall material. The regions with more cell-wall material (less lumen space) have more buckling resistance and will have a crushing or com-

TABLE 1. *Summary of microscope measurements (average of 50 measurements).*

	Ray width (μm)	Cell wall thickness		% Cell wall material	% Vessels
		Vessels (μm)	Fibers (μm)		
Maple	35	2.3	5.3	63	14
Oak EW	259	5.6	5.1	32	60
Oak LW	259	6	9	61	6

	% of total volume			
	Vessels	Fibers	Rays	Axial parenchyma
Acer saccharum[*]	21	61	17.9	0.1
Quercus rubra[**]	19.5	41.3	15.9	23.4

[*] Panshin, A. J. and C. de Zeeuw. 1980.
[**] Maeglin 1976.

pression type of failure. The regions with less cell-wall material (more lumen space) can easily become unstable and will tend to buckle or wrinkle. Table 1 clearly shows that oak EW is composed mostly of lumen space (68% of total volume) while oak LW and maple have relatively small amounts of lumen space and thus much more cell-wall material, 39% and 37% respectively. According to previous studies, vessels occupy 19.5% of the total volume of northern red oak (Maeglin 1976) and 21% of hard maple (Panshin and de Zeeuw 1980). Experimental measurements of vessel percentages in our maple samples indicate that vessels occupy 14% of the total volume of the maple specimens, which is slightly lower than the textbook values. Further, our measurements indicate that vessels are 60% of the volume of red oak EW and only 6% of red oak LW. Hence, these measurements support the assumption that less cell-wall material (more lumen space) will tend to buckle and the observation of red oak EW buckling failures, red oak LW crushing, and maple crushing failures.

Measurements of ray widths were made for both species to quantify the size and contribution of the rays. From Table 1 it is easy to see that the maple rays were very narrow compared to the wide oak rays. Comparison of experimental measurements indicates that our measurements were within the textbook values of 150–400 plus μm for red oak and from

uniserate to multiseriate in hard maple (Panshin and de Zeeuw 1980). Because the oak rays are so wide, they represent a broad plane of weakness in the wood—hence they are less strong and cause an irregularity in the structure. Due to the vector forces from the circular bolt loading, the Poisson effect, the irregularities of the rays that cause stress concentrations, and weakness of wood when loaded perpendicular to the grain, oak wood loaded in compression parallel to the grain will tend to fail in tension perpendicular to the grain. Therefore, our measurements support the observation that the rays in oak influenced the failure mode.

Bearing stress

Maximum load and displacement, bearing stress, and stiffness data are displayed in Table 2. Specific load was used to calculate bearing stress to minimize or eliminate the influence of specific gravity on the results. The amount of stress created by the bearing of the bolt on the surface of the wood is called the bearing stress. Bearing stress is obtained by dividing the specific load P by the area of the bolt in contact with the wood surfaces and is calculated as

$$\sigma_b = P/(td) \qquad (2)$$

where

TABLE 2.   Full-size bolt test results.

Specimen no.	Max. load		Max. bolt displacement		Specific bearing stress[*]		Specific stiffness in compression[**]	
	Maple (kg)	Oak (kg)	Maple (mm)	Oak (mm)	Maple (MPa)	Oak (MPa)	Maple (MPa)	Oak (MPa)
1	4,462.8	3,827.2	5.94	5.16	115	109	1,259	1,691
2	4,303.9	3,931.6	6.35	3.30	111	112	1,245	1,684
3	4,885	4,235.8	6.35	3.61	126	121	1,283	1,732
4	4,658	4,204	6.35	4.45	120	120	1,331	1,722
5	4,540	4,117.8	5.31	3.94	117	118	1,357	1,649
6	4,553.6	3,809.1	5.77	5.77	118	109	1,495	1,420
7	4,549.1	3,554.8	5.41	4.80	117	101	1,410	1,189
8	4,313	3,822.7	5.56	6.12	111	109	1,320	1,411
9	4,426.5	4,058.8	5.36	4.22	114	116	1,310	1,422
Ave.	4,533	3,938	6	5	117	112	1,338	1,562
SD	175	218	0	1	5	6	78	186
CV (%)	4	6	7	20	4	6	6	12

[*] Specific Bearing Stress = P/(t × d) where P = specific load (load/specific gravity); Oak = 0.57, Maple = 0.63; t = thickness of test specimen in contact with bolt; d = diameter of bolt.
[**] Stiffness in Compression = P/d where P = specific load at proportional limit; (load/specific gravity); d = bolt displacement at proportional limit.

P = the specific load (load ÷ the specific gravity)

t = the thickness of the test specimen in contact with the bolt

d = the diameter of the bolt.

A statistical t-test at a 95% confidence interval was performed on the mean specific loads to determine if the two species were statistically significantly different from one another. Through the t-test it was determined that the mean specific load and therefore, the bearing stress, of oak was *not significantly different* from maple. Based on this finding for the wood specimens used in this study, it can be concluded that the hardwood anatomical features did not influence the bearing stress.

Stiffness in compression

Specific stiffness in compression, defined as specific load (load ÷ specific gravity) divided by displacement of the bolt, was calculated at the proportional limit for each specimen. The displacement of the bolt was measured as the movement of the crosshead and was obtained from the load-displacement plots. These results are tabulated in Table 2. A statistical t-test at a 95% confidence interval was performed on the mean stiffnesses to determine

if the two species were statistically significantly different from one another. Through the t-test, it was determined that the mean stiffness of oak was *significantly different* from maple. Based on this finding, it can be concluded for the specimens used in that study that in contrast to the bearing stress, the hardwood anatomical features did influence the stiffness in compression.

It can also be seen from Table 2 that the oak specimens exhibited a higher coefficient of variability in the displacements than the maple specimens. The cause for the variable displacements observed within the oak specimens is most likely due to the irregular structure of oak and the mixed-mode failures, while the regular structure and failure mode of maple is probably the cause for the observed uniform displacements in maple.

Micromechanics tests of individual growth ring regions

Values for maximum load and specific crushing stress (normalized by specific gravity) from individual growth rings are shown in Table 3. Statistical t-tests at a 95% confidence interval indicate that the means for the maple specimens *were not* statistically significantly different from the oak LW values; however,

TABLE 3.   Micromechanics compression test results.

| Specimen no. | Max. load | | | | | |
| | | Oak | | | Oak | |
	Maple (kg)	EW (kg)	LW (kg)	Maple (MPa)	EW (MPa)	LW (MPa)
1	7.7	2.7	6.8	52.60	19.17	56.60
2	6.8	2.7	6.8	47.09	25.09	48.19
3	5.9	4.1	6.4	50.19	31.16	35.50
4	8.6	3.2	11.4	51.98	16.82	86.31
5	7.7	3.2	8.6	53.15	18.41	62.46
6	5.9	5.0	10.0	48.60	27.09	55.08
7	5.0	2.7	6.8	48.46	15.99	60.39
8	7.3	5.0	5.4	46.60	32.82	38.19
9	5.9	2.3	5.0	44.54	19.17	35.16
10	5.9	3.2	5.4	48.74	17.03	28.68
Sp. G.				0.59	0.46	0.65
Ave.	7	3	7	49	23	53
SD	1	1	2	3	6	15
CV (%)	16	28	27	6	26	29

* Crushing stress = P/A where P = specific maximum load (load/specific gravity); A = gross cross-sectional area.

the oak EW results *were* statistically significantly different from both maple and oak LW values. In all cases, maximum load and crushing stress for oak EW was almost half that of the maple and oak LW. Variability of the oak results was approximately equal and much higher than that of the maple specimens. Extreme care was taken in preparing these small specimens; however, the cross-sectional dimensions of the specimens were very close to the width of the earlywood portion of the growth rings in the initial test blocks and preparation artifacts were impossible to avoid. Also, an adjustable ball-and-socket assembly was not available for applying the load, so preparation artifacts and eccentricities in loading are the most probable sources of the high degree of variability.

However, the average values obtained with the micromechanics specimens compare well with previously published values for full-size specimens. The experimentally determined average value for the maple samples—49 MPa— compares very well with the handbook value (USDA-FS 1987) of 54 MPa for hard maple (sugar maple), specific gravity 0.63, and a

FIG. 6.   Photograph of buckling failure exhibited by oak earlywood microtest specimens. 12.5×.

moisture content of 12%. The maximum crushing stress handbook value (USDA-FS 1987) for northern red oak, specific gravity 0.59, 12% moisture content is 42 MPa, while the average experimental value for oak EW is 23 MPa and for oak LW is 53 MPa.

Observations of the failure patterns of the microspecimens indicate that they failed in the exact same manner as their respective full-size bolt specimens—the maple tended to crush,
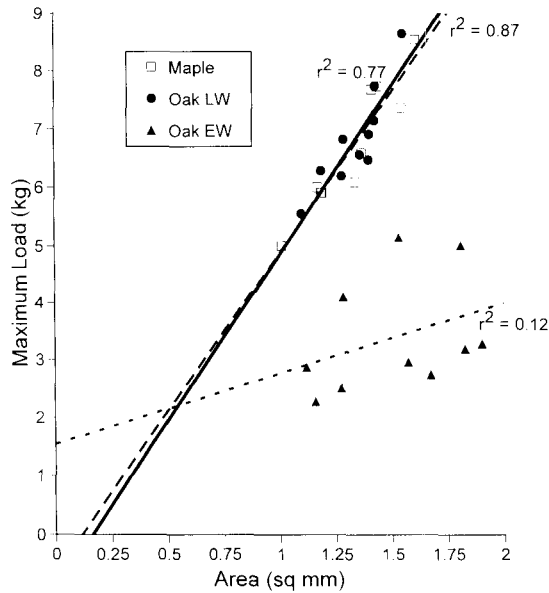
FIG. 7. Plot of maximum load versus cross sectional area for microtest specimens.

the oak EW dramatically buckled (see Fig. 6 for an example), and the oak LW tended to crush rather than visibly buckle. The much lower crushing strength of the oak EW and the tendency of the microtest specimens to duplicate failure modes give further explanation for the observed tendency of the earlywood portion of the full-size bolt specimens to buckle rather than crush.

Figure 7 shows a plot of the maximum load as a function of gross cross-sectional area for the micromechanical specimens. Regression coefficients for the maple specimens (r^2 = 0.87) and the oak LW (r^2 = 0.77) are very high; which indicates that the maximum load is strongly dependent on the cross-sectional area under load for the maple and oak LW specimens as expected for the elastic region. However, the r^2 value for the oak EW specimens is quite low (0.12). As mentioned previously, preparation artifacts were impossible to avoid with the oak EW specimens, and the lack of correlation is probably a result of high variability during specimen preparation. In addition, these specimens consisted of only a few large earlywood vessels surrounded by a few other cell elements (refer

to Fig. 1a). The tendency toward instable buckle failures (refer to Fig. 6) could explain the lack of correlation between ultimate load and gross cross-sectional area.

Micromechanics properties determined with the very small specimens can be used to calculate an average value for crushing strength of the full-size oak specimens using the law of mixtures. The overall average value for full-size crushing strength is calculated as the weighted average of the stress experienced by each growth ring layer as follows:

$$\sigma_w = \frac{(\sigma_{EW})(A_{EW}) + (\sigma_{LW})(A_{LW})}{(A_W)} \quad (3)$$

where

σ_w = crushing strength (stress) for the whole, full-size specimens

σ_{EW} = crushing strength of oak earlywood determined from microtest specimens

σ_{LW} = crushing strength of oak latewood determined from microtest specimens

A_{EW} = area of entire earlywood portion of bolt bearing area × bolt diameter

A_{LW} = area of entire latewood portion of bolt bearing area × bolt diameter

A_W = area of bolt bearing area (thickness of specimen in contact with bolt × diameter of bolt).

Using the values for maximum crushing stress for the micromechanics specimens from Table 3 and the average area of earlywood and latewood portions of the full-size oak specimens (0.017 m² and 0.045 m², respectively), the calculated value for the entire full-size oak specimens would be 38.5 MPa. This value compares well with the handbook value of 42 MPa (USDA-FS 1987) for northern red oak, specific gravity 0.59, 12% moisture content. While the value of maximum crushing stress calculated using the theory of mixtures compares well with the published value for northern red oak, this does not offer any proof necessarily.

CONCLUSIONS

This study focused on evaluating the influence of different hardwood anatomical features on the failure mode, bearing stress, and stiffness in compression of hard maple and red oak single-bolted connections. Based on the results obtained from the experiments and the above discussion, the following conclusions can be drawn:

- The uniform failure mode of maple may be attributed to its uniform anatomical structure, while the variable failure modes of oak may be attributed to its variable anatomical structure.
- Maple specimens and oak LW regions both displayed a crushing failure mode, while the oak EW regions showed a buckling failure mode. These observations can be attributed to the amount of cell-wall material and buckling resistance. Regions with more cell-wall material relative to lumen void space (oak LW and maple) will tend to crush, while regions mostly composed of lumen space (oak EW) will tend to buckle.
- The numerous, random cracks in oak were caused by the large, numerous rays failing in tension perpendicular to the grain, vector forces from the circular dowel loading, and to a lesser extent, the Poisson effect underneath the bolt.
- The variable amount of bolt displacement in oak compared to the constant amount of bolt displacement in maple was caused by the irregular structure of oak and uniform structure of maple.
- Bearing stress was not influenced by different hardwood anatomical features; however, stiffness in compression was and this influence should be considered in future design specifications.

ACKNOWLEDGMENTS

REFERENCES

AMERICAN FOREST AND PAPER ASSOCIATION. (AFPA) 1991. National design specifications for wood construction. Washington, DC. 125 pp.

AMERICAN SOCIETY FOR TESTING AND MATERIALS. (ASTM) 1986a. ASTM Standard D-2016-83 Standard test methods for moisture content of wood. Method A, Ovendry Method. Philadelphia, PA.

————. 1986b. ASTM Standard D-2395-83. Standard test methods for specific gravity of wood and wood-based materials. Philadelphia, PA.

————. 1993. Standard test methods for mechanical fasteners in wood. ASTM D 1761. Annual Book of Standards, Section 4, Volume 4.09, 1993. Philadelphia, PA.

BARISKA, M., AND L. J. KUCERA. 1985. On the fracture morphology of wood. Part 2: Macroscopical deformations upon ultimate axial compression in wood. Wood Sci. Technol. 19(1):19–34.

BODIG, J. 1965. The effect of anatomy on the initial stress-strain relationship in transverse compression. Forest Prod. J. 15(5):197–202.

————, AND B. A. JAYNE. 1982. Mechanics of wood and wood composites. New York, NY. Van Nostrand Reinhold, xxi, 712 pp.

CHOI, D., J. L. THORPE, W. A. CÔTÉ, AND R. B. HANNA. 1996. Quantification of compression failure propagation in wood using digital image pattern recognition. Forest Prod. J. 46(10):87–93.

CÔTÉ, W. A., AND R. B. HANNA. 1983. Ultrastructural characteristics of wood fracture surfaces. Wood Fiber Sci. 15(2):135–163.

FANTOZZI, J., AND P. E. HUMPHREY. 1995. Effects of bending moments on the tensile performance of multiple-bolted timber connectors. Part 1: A technique to model such joints. Wood Fiber Sci. 27(1):55–67.

HILSON, B. O., L. R. J. WHALE, D. J. POPE, AND I. SMITH. 1987. Characteristic properties of nailed and bolted joints under short-term lateral load. Part 3: Analysis and interpretation of embedment test data in terms of density related trends. J. Inst. Wood Sci. 11(2):65–71.

HUMPHREY, P. E., AND L. J. OSTMAN. 1989a. Bolted timber connections. Part 1: A wafer technique to model wood deformation around bolts. Wood Fiber Sci. 21(3):239–251.

————, AND ————. 1989b. Bolted timber connections. Part II: Bolt bending and associated wood deformation. Wood Fiber Sci. 21(4):354–366.

KERMANI, A., AND W. M. C. MCKENZIE. 1994. The use of single-beam reflection holography to determine strain distributions around bolts. J. Instit. Wood Sci. 13(4):454–458.

KUCERA, L. J., AND M. BARISKA. 1982. On the failure morphology in wood. Part 1: A SEM-study of deformations

in wood of spruce and aspen upon ultimate axial compression load. Wood Sci. Technol. 16(1982):241–259.

JOHANSEN, K. W. 1949. Theory of timber connections. International Association for Bridge and Structural Engineering. Vol. 9, pp. 249–262.

LARSEN, H. J. 1992. Eurocode Overview. Presentation at FPRS International Workshop on Wood Connections, November, 1992, Las Vegas, NV.

LHUEDE, E. P. 1987. Loads in bolted timber joints stressed perpendicular to the grain. J. Inst. Wood Sci. 11(2):17–25.

MCLAIN, T. E., AND S. THANGJITHAM. 1983. Bolted wood-joint yield model. J. Struct. Eng. 109(8):1820–1835.

MAEGLIN, R. R. 1976. Natural variation of tissue proportions and vessel and fiber lengths in northern red oak. Silvae Genet. 25(3/4):122–126.

PANSHIN, A. J., AND C. DE ZEEUW. 1980. Textbook of wood technology. 4th ed. McGraw-Hill Book Company, New York, NY. 722 pp.

RAHMAN, M. U., Y. J. CHIANG, AND R. E. ROWLANDS. 1991. Stress and failure analysis of double-bolted joints in Douglas-fir and Sitka spruce. Wood Fiber Sci. 23:567–589.

ROWLANDS, R. E., M. U. RAHMAN, T. L. WILKINSON, AND Y. I. CHIANG. 1982. Single- and multiple-bolted joints in orthotropic materials. Composites 13(3):273–279.

SALINEKOVICH, A., J. R. LOFERSKI, AND A. G. ZINK. 1996. Understanding the performance of laterally loaded wood connections assembled with multiple bolts. Forest

Products Society, Madison, WI. Wood Design Focus. 7(4):19–26.

SCHNEIWIND, A. P. 1959. Transverse anisotropy of wood. Forest Prod. J. 9(10):350–359.

SOLTIS, L. A., F. K. HUBBARD, AND T. L. WILKINSON. 1986. Bearing strength of bolted timber joints. J. Struct. Eng. 112(9):2141–2153.

STELMOKAS, J. W., A. G. ZINK, AND J. R. LOFERSKI. 1997. Image correlation analysis of multiple bolted wood connections. Wood Fiber Sci. 29(3):210–227.

TRAYER, G. W. 1932. The bearing strength of wood under bolts. Technical Bulletin No. 332. USDA. Washington, DC. 40 pp.

UMBAUGH, S. E. 1998. Computer vision and image processing: A practical approach using CVIPtools. Prentice Hall, Upper Saddle River, NJ. 504 pp.

USDA FOREST SERVICE. 1987. Wood handbook: USDA Agric. Handb. 72 (rev.) USDA Forest Service, Forest Prod. Lab., Madison, WI. 466 pp.

WONG, C. M. S., AND F. L. MATTHEWS. 1981. A finite element analysis of single and two-hole bolted joints in fibre reinforced plastic. J. Composite Mater. 14:481–491.

WILKINSON, T. L., AND R. E. ROWLANDS. 1981. Analysis of mechanical joints in wood. Exp. Mech. 21(11):408–414.

ZINK, A. G., R. W. DAVIDSON, AND R. B. HANNA. 1995. Strain measurement in wood using a digital image correlation technique. Wood Fiber Sci. 27(4):346–359.